A Computational Foray into the Mechanism and Catalysis of the Adduct Formation Reaction of Guanine with Crotonaldehyde

Asja A. Kroeger, and Amir Karton *

Crotonaldehyde, a common environmental pollutant and product of endogenous lipid peroxidation, reacts with guanine to form DNA adducts with pronounced genotoxicity and mutagenicity. Here, we explore the molecular mechanism of this adduct formation using double-hybrid density functional theory methods. The reaction can be envisaged to occur in a two-step fashion via an aza-Michael addition leading to an intermediate ring-open adduct followed by a cyclization reaction giving the mutagenic ring-closed adduct. We find that (i) a 1,2-type addition is favored over a 1,4-type addition for the aza-Michael addition, and (ii) an initial tautomerization of the guanine moiety in the resulting ring-open adduct significantly reduces the barrier toward cyclization compared to the direct cyclization of the ring-open adduct in its keto-form. Overall, the aza-Michael addition is found to be rate-determining. We further find that participation of a catalytic water molecule significantly reduces the energy barriers of both the addition and cyclization reaction. © 2018 Wiley Periodicals, Inc.

DOI:10.1002/jcc.25595

Introduction

DNA damage by endogenous or exogenous chemical agents plays an important part in the development and progression of a wide range of conditions including cancer [1], inflammation [2], diabetes [3], and neurodegenerative diseases [4,5]. Reactive aldehyde species have been found to react readily with DNA bases, in particular guanine, to form adducts that may disrupt base pairing, form DNA crosslinkers or react with proteins and peptides [6].

Crotonaldehyde is a volatile and lipophilic α,β-unsaturated aldehyde that has been widely studied with respect to the disease promoting activities of its adducts with the DNA base guanine [6–8]. It has been found to be mutagenic in bacteria [9] as well as to cause liver tumors in rats [10]. In vitro studies by Czerny et al. [11] further found a pronounced genotoxicity and mutagenicity of its DNA adducts in human lymphoblast cells. Introduction of the adducts into the DNA of human xeroderma pigmentosum cells by Stein et al. [12] resulted miscoding frequencies of 5% and 10% for the two observed diastereomeric adducts suggesting the adducts play a significant role in human carcinogenesis and aging.

Exposure to crotonaldehyde may result both from endogenous and exogenous sources. It is well known as a product of endogenous lipid peroxidation as a result from oxidative stress [13–15] as well as a common environmental contaminant from sources such as cigarette smoke [16] and automobile emissions [17]. It has further been postulated that crotonaldehyde may be formed in vivo after alcoholic beverage consumption via polyamine catalyzed aldol condensations of the primary alcohol metabolite acetaldehyde [18,19]. This is of particular interest as it may offer an explanation to the currently insufficiently understood strong association between alcohol consumption and the development of gastrointestinal cancers [18,19].

The reaction of crotonaldehyde with guanine may form a ring-open and a ring-closed adduct via an initial addition reaction and subsequent cyclization step (illustrated in Scheme 1a). While the ring-open adduct is mainly found in double-strand DNA, the ring-closed form predominates in single-strand DNA [19,20]. Based on its miscoding potency it has been proposed by Minko et al. [6] that at the replication fork the adduct exists in its ring-closed form. Scheme 1b shows that in the mutagenic ring-closed adduct Watson–Crick base pairing is significantly disrupted while the ring-open adduct maintains a reactive aldehyde group that has been found to further react with DNA bases, proteins and peptides to form crosslinkers [21,22].

While numerous experimental studies have examined the biological activities of reactive aldehydes as well as the properties of their DNA adducts [6,15], there has been little research into the molecular mechanisms of adduct formation. A detailed knowledge of the reaction mechanism is important for predicting the mutagenicity of a wide range of Michael acceptors of biological relevance [23]. Computational studies by Pardo et al. [24] and more recently by Desmet et al. [25] explored the mechanism of the aza-Michael reactions between small

[a] A. A. Kroeger, A. Karton
School of Molecular Sciences, The University of Western Australia, Perth, Western Australia, 6009, Australia
E-mail: amir.karton@uwa.edu.au

National Computational Infrastructure (NCI), which is supported by the Australian Government; Forrest Research Foundation Scholarship and an Australian Government Research Training Program Stipend (to A.A.K.); Australian Research Council (ARC) Future Fellowship (to A.K.; Project No. FT170100373).
Contract Grant sponsor: Australian Research Council; Contract Grant number: FT170100373; Contract Grant sponsor: University of Western Australia

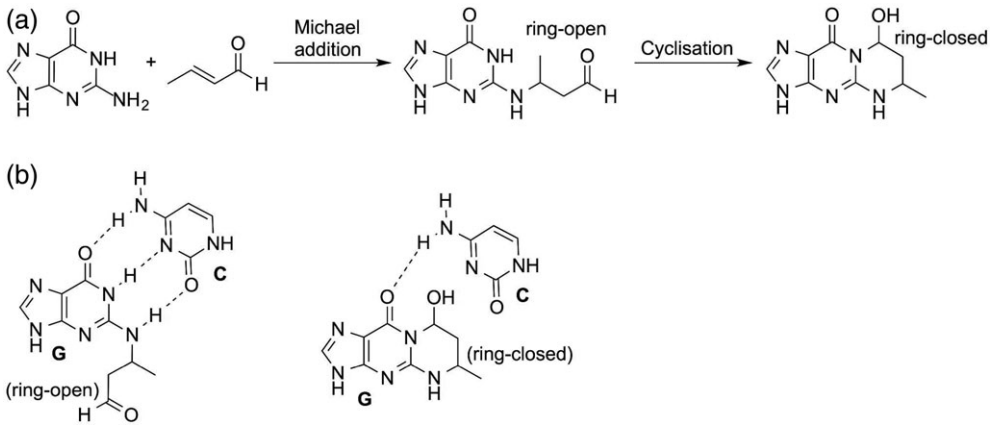

Scheme 1. a) A schematic representation of the two-step formation of the DNA adduct between guanine and crotonaldehyde. b) The effect of the ring-open (left) and ring-closed (right) adduct on Watson–Crick base pairing.

exemplary aldehydes and amines. While Pardo et al. concluded that a 1,4-type mechanism is favored [24], Desmet et al. found that due to high barriers toward tautomerization of the enol intermediate of the 1,4-addition, a direct 1,2-type addition pathway is kinetically favorable [25]. To the best of our knowledge, the only previous computational investigation into the reaction mechanism of a DNA adduct formation was carried out by Xing et al. [26] on the reaction of guanine with trans-4-hydroxy-2-nonenal (4-HNE). The authors explored the commonly postulated mechanism of a 1,4-type Michael addition followed by cyclization via a nucleophilic addition using density functional theory (DFT). They found high reaction barriers of 229.7 and 234.7 kJ mol^{-1} for the uncatalyzed conjugate addition and cyclization steps, respectively. They also found that participation of a catalytic water molecule in the tautomerization of the enol intermediate in the conjugate addition reduces the barrier for this step to 113.5 kJ mol^{-1}.

In the present work, we use double-hybrid DFT (DHDFT) to investigate the mechanism of formation of the ring-open and ring-closed adducts between guanine and crotonaldehyde. We explore two different pathways for both the aza-Michael addition as well as the cyclization reaction and show that a catalytic water molecule can significantly reduce the activation energies of most steps in the reaction pathways under consideration. We find that the previously unexplored 1,2-type addition and a tautomerization of the nucleobase in the ring-open adduct prior to cyclization are notably favorable over the 1,4-type addition and direct cyclization. Unlike previously reported, the conjugate addition emerges as rate-determining. Scheme 2 illustrates our proposed mechanism for the aza-Michael addition and cyclization steps.

Computational Methods

The geometries of all structures along the potential energy surfaces (PESs) were optimized in the gas phase using the B3LYP-D3 exchange-correlation DFT functional [27–29] with the 6-31+G (2df,p) basis set [30–32]. Zero-point vibrational energy and enthalpic corrections have been obtained from such calculations. Equilibrium and transition structures were verified via frequency calculations. The intrinsic reaction coordinate [33,34] was calculated for all transition structures to confirm the connectivity of transition structures to the related products and reactants.

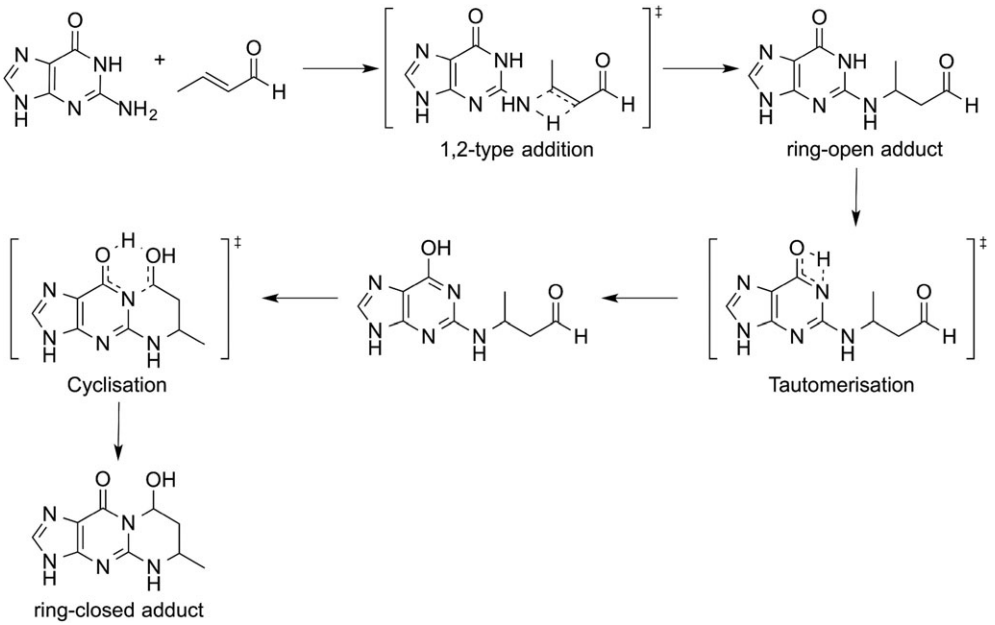

Scheme 2. Schematic representation of the proposed mechanism for the adduct formation between crotonaldehyde and guanine.

Double-hybrid density functional theory single-point energy calculations at the DSD-PBEP86/Def2-TZVPP level of theory were performed on the B3LYP-D3/6-31+G(2df,p) optimized geometries [35,36]. Corrections for bulk solvent effects in aqueous solution were calculated using the SMD continuum solvation model at the M05-2X/6-31G(d) level of theory [37] and added to the DSD-PBEP86/Def2-TZVPP energies. For a number of reaction profiles we optimized the geometries in aqueous solution at the SMD(water)-B3LYP-D3/6-31+G(2df,p) level of theory. This does not lead to significant variations in the final reaction profiles and the qualitative trends are unchanged (for further details see the Supporting Information). All geometry optimizations and single-point energy calculations were performed using the Gaussian09 and Gaussian16 software packages [38,39]. To assist in rationalizing differences in stability between the various conformations of the ring-closed adduct, natural bond orbital (NBO) calculations [40–42] were performed at the B3LYP/6-31G(d,p) level of theory using the NBO6 [43] and Gaussian09 program packages and stabilization energies resulting from second-order perturbation theory analysis, referred to as $E^{(2)}$ energies, are reported. All 3D structural representations were generated using CYLview [44].

Results and Discussion

As illustrated by Scheme 1a, the adduct formation reaction may be broken down into two steps, an aza-Michael addition and a cyclization step. For clarity, the discussion here will be separated accordingly.

Aza-Michael addition

For the conjugate addition two pathways can be envisaged, one in which the addition occurs concomitant with a 1,2-type proton transfer between the nitrogen of the 1° amine and the alpha-carbon, directly leading to the keto product. Alternatively, the addition may be concomitant with a 1,4-proton transfer between the nitrogen of the 1° amine and the carbonyl oxygen leading to an enol intermediate. For this enol-intermediate reaction of the s-trans rotamer of crotonaldehyde leads to an E-configuration in the newly formed double bond whereas reaction with s-cis crotonaldehyde gives a Z-conformation. Subsequent tautomerization of the enol-intermediate leads to the keto-tautomer of the ring-open adduct. A schematic representation of the transition structures of the addition step on the example of s-cis crotonaldehyde is shown in Scheme 3. We note in passing that we also considered the uncatalyzed and water-catalyzed 1,2- and 1,4-addition between crotonaldehyde and the enol-tautomer of guanine. However, the resulting aromaticity of the pyrimidine appears to have little effect on the reaction barriers. The absence of the NH group in alpha-position in the enol-tautomer further precludes the stabilizing hydrogen-bonding interaction with the aldehyde carbonyl oxygen in the 1,2-addition (Supporting Information Tables S1–S5 give the energies of the structures along those pathways).

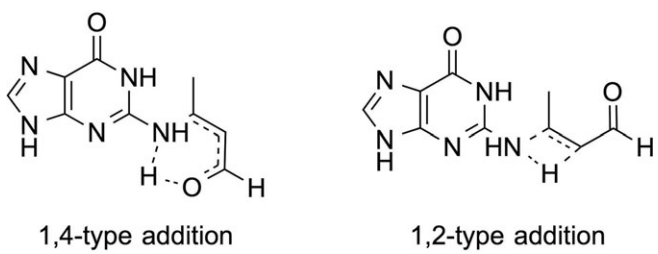

Scheme 3. Schematic representation of the transition structures associated with the 1,4-type (left) and the 1,2-type (right) addition pathways under consideration.

Water is a well-known proton-transfer catalyst [45–54] and abundant in the biological system. It can be envisaged that participation of an explicit water molecule in all steps of both pathways may facilitate the proton transfers, thereby lowering energy barriers toward the transformations. Figure 1 gives the potential energy surfaces for the uncatalyzed (a) and water-catalyzed (b) aza-Michael addition step of the adduct formation reaction along with the geometries of the respective transition structures.

While for the catalyzed pathways transition structures resulting from s-cis as well as s-trans crotonaldehyde could be located, for the uncatalyzed 1,4-type addition a transition

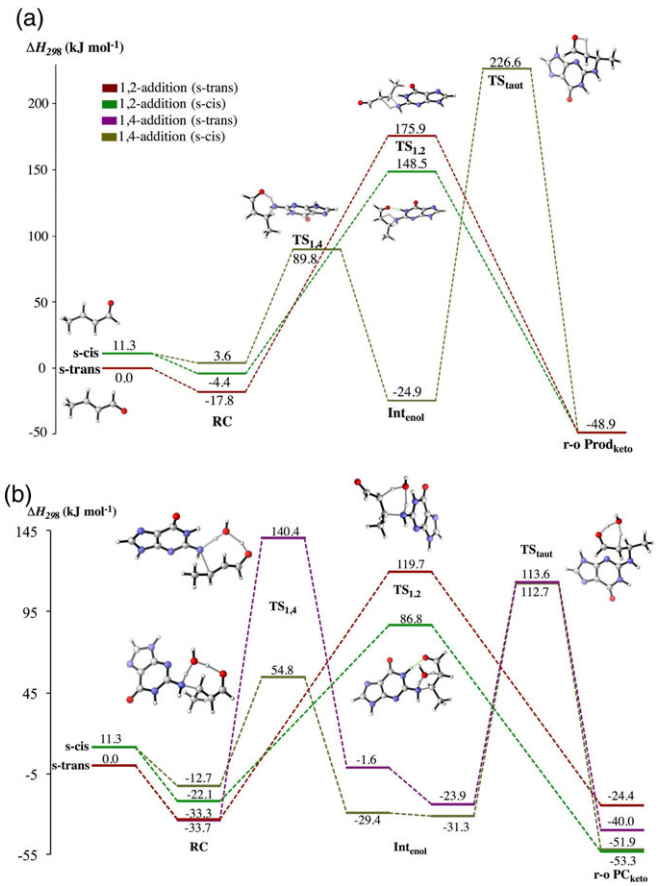

Figure 1. Reaction profiles (DSD-PBEP86-D3/Def2-TZVPP, ΔH_{298}, kJ mol^{-1}) for the uncatalyzed (**a**) and water-catalyzed (**b**) aza-Michael addition step. The energies of the reactants, reactant complexes (RC), transition structures (TS), intermediates, and ring-open (r-o) product complexes (PC) are given relative to the free reactants. Atomic color scheme: H, white; C, gray; N, blue; O, red. The bonds being broken and formed in the transition structures are represented by gray lines, H-bonds are represented by green lines. [Color figure can be viewed at wileyonlinelibrary.com]

structure could only be located for the reaction with the s-cis rotamer of crotonaldehyde. Overall, it is observed that transition structures resulting from s-cis crotonaldehyde are vastly preferred. We note that the interconversion between s-trans and s-cis crotonaldehyde occurs with a fairly low energy barrier of $\Delta H_{298}^{\ddagger}$ = 37.2 kJ mol^{-1} calculated at the DSD-PBEP86-D3/Def2-TZVPP level of theory. Both for the uncatalyzed and the catalyzed reaction, the concerted 1,2-type pathway is favored resulting in barriers of 152.9 (uncatalyzed) and 108.9 kJ mol^{-1} (water-catalyzed) relative to the reactant complexes (Fig. 1). In the 1,4-type addition pathways the reaction barriers for the initial addition steps (89.8 and 67.5 kJ mol^{-1}, respectively for the uncatalyzed and water-catalyzed pathways) are significantly lower than those of the concerted 1,2-addition. Both tautomerization steps, however, give prohibitively high barriers of 226.6 (uncatalyzed) and 146.4 (catalyzed) kJ mol^{-1}, making the overall pathway unfavorable.

Many of the observed trends can be rationalized on further inspection of the geometries of the transition structures. Whereas the uncatalyzed 1,4-addition step occurs via a favorable 6-membered transition structure, the 1,2-type addition occurs via a strained 4-membered ring transition structure. Accordingly, the proton transfer trajectories of the uncatalyzed 1,2-addition are at ∠N-H-C = 111.3° (s-cis) and 112.3° (s-trans) much further from an ideal linear trajectory than the ∠N-H-O = 156.0° observed for the 1,4-addition.

Water catalysis expands the cyclic transition structures to eight- (1,4-addition) and six-membered (1,2-addition) rings, reducing ring-strain and optimizing proton transfer trajectories. Now the 1,4-type addition leads to near-linear trajectories of ∠N-H-O = 170.9° and ∠O-H-O = 170.6° (s-cis) while the 1,2-addition pathway leads to notably improved trajectories of ∠N-H-O = 159.8° and ∠O-H-C = 153.6° (s-cis). It is instructive to note that the higher energy transition structures resulting from s-trans crotonaldehyde generally show poorer proton transfer trajectories of ∠N-H-O = 169.5° and ∠O-H-O = 155.5° (1,4-addition) and ∠N-H-O = 144.5° and ∠O-H-O = 158.1° (1,2-addition).

The uncatalyzed tautomerization step of the 1,4-addition pathway proceeds via a highly strained 4-membered transition structure, meaning the proton transfer occurs at an unfavorable angle of 104.6°. Although participation of a catalytic water molecule expands the cyclic transition structures to more relaxed 6-membered rings, the proton transfer trajectories observed are at ∠N-H-O = 145.7° and ∠O-H-O = 156.6 still notably less linear than those observed for the favorable addition steps, partially explaining why a pathway including tautomerization is unlikely.

The Newman projections of the reaction centers of the different transition structures for the addition steps depicted in Figure 2 allow further insights into why differing stabilities are observed for the different conformations and pathways. It was previously found that the steric effects of a staggered or eclipsed conformation in the transition structure can have a significant influence on the pathway selectivity of a reaction [55–57]. In the addition reaction here the transition structures pertaining to the 1,4-addition with s-cis crotonaldehyde, both for the uncatalyzed and the water-catalyzed pathway, are in a favorable staggered conformation and accordingly give the lowest barriers in the pathways of 86.2 and 67.5 kJ mol^{-1}, respectively (relative to the reactant complex). The same reaction via s-trans crotonaldehyde results a sterically hindered eclipsed transition structure. Accordingly, an increase in activation energy of 106.6 kJ mol^{-1} is observed. The higher energy transition structures of the 1,2-addition largely yield sterically hindered eclipsed geometries. Unlike the transition structures resulting from the s-trans rotamer, those pertaining to the reaction of the s-cis rotamer allow for a stabilizing hydrogen-bonding interaction between the carbonyl and the 2° amine of the pyrimidine (Fig. 2), rationalizing the higher stability of the s-cis-like transition structures.

Further, it can be observed that for both the uncatalyzed and the catalyzed reaction the forming C···N bond is longer in transition structures resulting from the s-trans rotamer as compared to those pertaining to the s-cis rotamer, indicating that the latter rotamer gives transition states that are later in the addition reaction. Whereas the s-trans rotamer results C···N bond lengths of 1.614 Å (uncatalyzed) and 1.629 Å (catalyzed), the s-cis rotamer gives a C···N bond length of 1.560 Å for both the uncatalyzed and catalyzed pathways.

Overall, the aza-Michael addition step will occur via a concerted 1,2-type addition leading directly to the ring-open adduct. Compared to the uncatalyzed reaction, participation of a catalytic water molecule reduces the activation energy of this step by 44.0 kJ mol^{-1}.

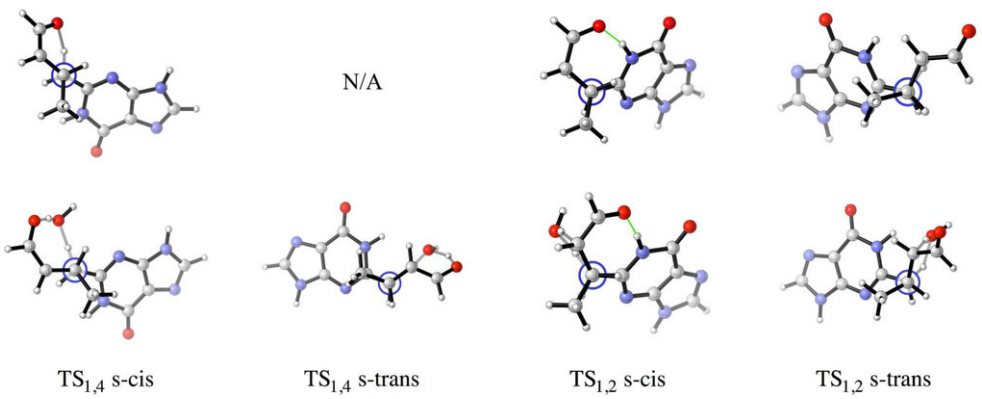

Figure 2. Newman projections of the reaction centers of the transition structures of the 1,4- and 1,2-addition steps (upper pane: uncatalyzed, lower pane: water-catalyzed). The bonds being broken and formed in the transition structures are represented by gray lines, H-bonds are represented by green lines. [Color figure can be viewed at wileyonlinelibrary.com]

Cyclization reaction

The cyclization of the ring-open adduct occurs via nucleophilic attack by the pyrimidine nitrogen in alpha position at the carbonyl carbon of the new aldehyde substituent and a proton transfer to the carbonyl oxygen. For this reaction two pathways are possible: One, in which the cyclization is preceded by a tautomerization of the guanine moiety in the ring-open adduct, giving the enol-tautomer of guanine and one in which the keto-form reacts directly. As illustrated by the schematic transition structures given in Scheme 4 this changes the substituents involved in the proton transfer. Whereas in the direct cyclization the proton transfer occurs between the pyrimidine nitrogen and the aldehyde carbonyl, the proton transfer in the reaction involving the enol-tautomer occurs between the enol hydroxyl group and the carbonyl.

Both the conjugate addition as well as the cyclization step form new stereocenters. In the cyclization step, the relative stereochemistry of the two stereocenters determines the possible orientations of the substituents on the forming 6-membered ring. As in the conjugate addition it can be envisaged that the proton transfers in all pathways may be catalyzed by an explicit water molecule.

Figure 3 gives schematic PESs for the uncatalyzed and water-catalyzed cyclization reaction of both the keto- and enol-tautomers of the ring-open starting material. For each tautomer, four different relative stereochemistries and substituent orientations are possible. For clarity Figure 3 only gives the PESs for those pathways that result in the lowest activation energy for this step (Tables S6–S9 of the Supporting Information give the energies of the transition structures leading to all possible conformations and configurations).

As illustrated in Figure 3, the direct cyclization of the ring-open adduct from its keto-form yields high barriers of 188.3 and 110.8 kJ mol^{-1} for the uncatalyzed and catalyzed reactions, respectively. Compared to this an initial tautomerization of the guanine moiety leads to significant overall barrier reductions of 26.6 (uncatalyzed) and 55.2 kJ mol^{-1} (catalyzed). With activation energies of 161.7 (uncatalyzed) and 55.6 kJ mol^{-1} (catalyzed), the tautomerization reactions of this pathway form the rate-determining steps of both reactions while the ensuing cyclizations give low barriers of 35.0 (uncatalyzed) and 38.6 (catalyzed) kJ mol^{-1}. Overall, water catalysis reduces the activation energy of the rate-determining step very significantly by 106.1 kJ mol^{-1}.

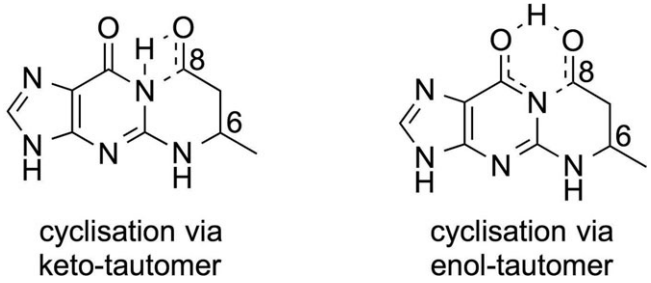

Scheme 4. Schematic representation of the transition structures associated with the direct cyclization via the keto-tautomer (left) and cyclization via the enol-tautomer (right).

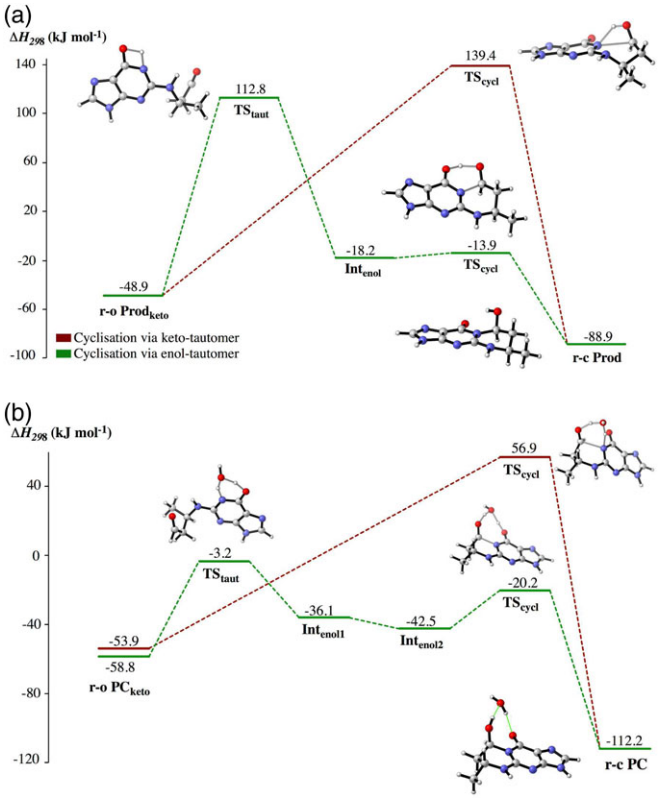

Figure 3. Reaction profiles (DSD-PBEP86-D3/Def2-TZVPP, ΔH_{298}, kJ mol^{-1}) for the uncatalyzed (**a**) and water-catalyzed (**b**) cyclization step. The energies of the initial ring-open (r-o) adducts, transition structures (TS), intermediates, and ring-closed (r-c) product complex (PC) are given relative to the free reactants in Figure 1. Atomic color scheme: H, white; C, gray; N, blue; O, red. The bonds being broken and formed in the transition structures are represented by gray lines, H-bonds are represented by green lines. [Color figure can be viewed at wileyonlinelibrary.com]

It is instructive to note that although participation of a catalytic water molecule reduces the activation energy of the direct cyclization of the keto-tautomer of the adduct by as much as 77.5 kJ mol^{-1}, this is not the case for the cyclization of the enol-tautomer where the barrier toward cyclization is marginally lower for the uncatalyzed reaction. These observations can largely be attributed to changes in the ring-sizes of the cyclic transition structures. In the cyclization of the keto-tautomer a strained 4-membered cyclic transition structure leads to both highly unfavorable trajectories for the proton transfer and the nucleophilic addition of ∠N-H-O = 126.7° and ∠N-C-O = 75.5°, respectively. Participation of the catalytic water molecule allows for a more relaxed six-membered ring. In particular, we obtain improved trajectories of ∠N-H-O = 160.5° and ∠O-H-O = 155.2° for the proton transfers, and ∠N-C-O = 107.4° for the nucleophilic addition. The cyclization of the enol-tautomer occurs concomitant with a proton transfer between the enol OH-group and the carbonyl, allowing for a favorable 6-membered cyclic transition structure in the uncatalyzed pathway. Near-ideal trajectories of ∠O-H-O = 157.0 and ∠N-C-O = 106.7 result for the proton transfer and nucleophilic addition. Participation of the water molecule here expands the transition structure to an 8-membered ring, which without giving a reduction in ring-

strain, leads to comparably smaller improvements in the trajectories of the proton transfer and nucleophilic addition.

It can be observed that in all transition structures pertaining to the pathways involving the enol-tautomer of the guanine moiety the forming N···C bond is notably shorter than in those transition structures containing the keto-tautomer indicating that in the transition states via the enol-tautomer the cyclization is more advanced. In the case of the pathways illustrated in Figure 3 the keto-tautomer leads to N···C bond lengths of 2.500 Å (uncatalyzed) and 2.147 Å (catalyzed) whereas the enol-tautomer gives N···C bond lengths of 1.840 Å (uncatalyzed) and 1.779 Å (catalyzed). This can partly be attributed to steric encumbrance from the carbonyl substituent of the guanine moiety at the reaction center.

It has been found that the ring-open adduct is mainly observed in double-stranded DNA whereas in single-stranded DNA the adduct is largely present in its ring-closed form [19,20,58]. The observations here can offer a plausible explanation for this. Tautomerization reactions of the DNA bases are expected to occur more readily in single-stranded DNA than in double-stranded DNA where the substituents are involved in Watson–Crick base pairing. The results presented here show that an initial tautomerization of the DNA base is necessary for a facile cyclization reaction. In double-stranded DNA, where tautomerization is unlikely only the high energy direct cyclization of the keto-adduct would be accessible making the reaction overall unlikely.

Due to conformational flexibility of the newly formed 6-membered ring and the formation of a new stereocenter the cyclization reaction may proceed via a number of conformationally different transition structures giving two different half-chair conformations and either the same (shown as R,R) or opposite stereochemistry (shown as R,S) at the two newly formed stereocenters at C6 and C8 (Scheme 4). The PESs in Figure 3 represent those pathways that resulted the most stable transition structures. As illustrated in Figure 3, in the uncatalyzed reaction these transition structures lead to a ring-closed adduct with opposite stereochemistry at C6 and C8. The methyl and hydroxyl group are cis to each other and both assume an equatorial orientation. When catalyzed, conversely, the most stable transition structure leads to an adduct in which C6 and C8 have the same stereochemistry. The substituents are trans and the methyl group has an equatorial orientation while the hydroxyl group is in an axial orientation.

Figure 4 illustrates the relative configurations for the two different half-chairs possible for the ring-closed adduct and their relative energies. Overall, we find that the first half-chair conformation (structures **a** and **b**) allowing for an equatorial methyl group gives the more stable adducts. Apart from the most favorable structure **a**, the conformations are all very close in energy. In structure **a**, C6 and C8 have the same stereochemistry leading to a trans relationship between the two substituents. The methyl group assumes an equatorial orientation while the hydroxyl group is in an axial orientation. In agreement with the results presented here, a conformational analysis of the same adduct using 2D NMR methods by Boerth et al. [59] finds the ring-closed adduct of conformation **a** to be present at 93.5%.

From conformational analyses of cyclohexanes it is well known that those conformations with bulky substituents in an equatorial orientation are thermodynamically favored [60]. While this can explain why structures **a** and **b** with equatorial methyl groups are more stable than structures **c** and **d**, the higher stability of structure **a** counters this. Consideration of competing electrostatic and stereoelectronic interactions may rationalize why an axial hydroxyl group is favorable. Table 1 gives overall dipole moments of the structures **a**–**d** as well as $E^{(2)}$ energies from second order perturbation analysis for the stabilizing negative $p_N \rightarrow \sigma^*_{C\text{-}O}$ hyperconjugation interaction between the

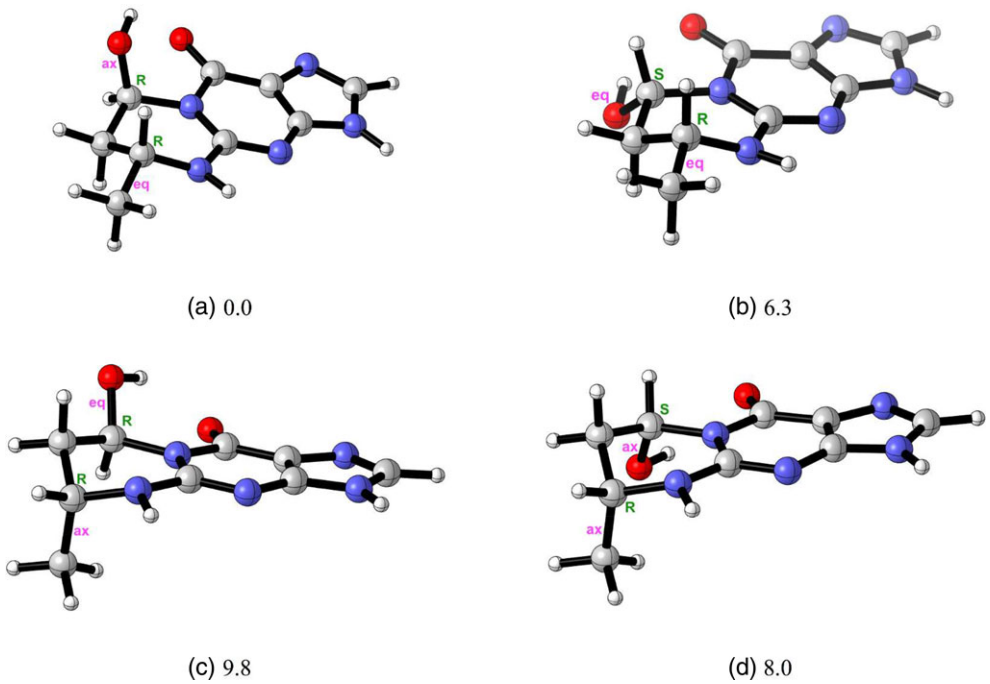

Figure 4. Conformations of the ring-closed adduct of guanine and crotonaldehyde and their relative energies (DSD-PBEP86-D3/Def2-TZVPP, ΔH_{298}, kJ mol^{-1}). Atomic color scheme: H, white; C, gray; N, blue; O, red. [Color figure can be viewed at wileyonlinelibrary.com]

Table 1. Total dipole moments (μ Debye) and $E^{(2)}$ $p_N \rightarrow \sigma^*_{C\text{-}O}$ energies in kJ mol^{-1} for all conformations of the ring-closed adduct of guanine and crotonaldehyde.

	a trans	b cis	c trans	d cis
μ	6.5	7.0	7.0	6.3
$E^{(2)}$ $p_N \rightarrow \sigma^*_{C\text{-}O}$	53.8	34.4	35.0	51.2

hydroxyl substituent and the neighboring nitrogen. We find that structures with an axial hydroxyl group (**a** and **d**) give lower overall dipole moments indicating smaller destabilizing electrostatic interactions. As the adducts are otherwise structurally the same, the orientation of the hydroxyl substituent is expected to largely determine differences in total dipole. Figure 4 illustrates that whereas the hydroxyl and the carbonyl group of the guanine moiety have different orientations in structures **a** and **d**, they have the same orientation in structures **b** and **c** meaning their dipoles are aligned and cause destabilizing repulsion. The stabilizing hyperconjugative $p_N \rightarrow \sigma^*_{C\text{-}O}$ interaction is ~33% higher in those structures with an axial hydroxyl group compared to those with an equatorial hydroxyl group. This indicates that an axial hydroxyl group leads to orbital orientations more favorable for stabilizing overlap than an equatorial hydroxyl group.

Conclusions

The mechanism and water catalysis of the adduct formation reaction between guanine and crotonaldehyde has been studied using DHDFT methods. We find that this reaction proceeds via two steps: an aza-Michael addition reaction giving a ring-open adduct followed by a cyclization reaction giving the ring-closed adduct. For each step, we considered two pathways. In the addition step a 1,4-type addition with subsequent tautomerization or a direct 1,2-type addition can be envisaged. Both for the uncatalyzed and water-catalyzed reactions, the 1,2-type addition, giving barriers of 152.9 (uncatalyzed) and 108.9 kJ mol^{-1} (catalyzed), is favorable due to a high barrier toward tautomerization observed for the 1,4-type addition.

The cyclization reaction can be envisaged to occur either via a direct nucleophilic addition and proton transfer from the pyrimidine nitrogen to the newly formed carbonyl or via a stepwise pathway in which nucleophilic addition is preceded by a tautomerization of the guanine. The following proton transfer consequently occurs between the reacting carbonyl and the hydroxyl group of the formed enol-tautomer of the guanine moiety. For both the uncatalyzed and catalyzed reaction the pathway via the enol-tautomer emerges as the kinetically favorable pathway. With barriers of 161.7 (uncatalyzed) and 55.6 kJ mol^{-1} (catalyzed) the initial tautomerization of the guanine moiety emerges as rate-determining for this step.

Interestingly, the rate-determining step for the formation of the final ring-closed product changes upon catalysis: While the cyclization step is rate-determining for the uncatalyzed adduct formation, the aza-Michael addition step is rate-determining in the catalyzed reaction. Overall, water is found to be a viable catalyst for the adduct formation, reducing the energy barriers toward the addition and cyclization reactions by 44.0 and 106.1 kJ mol^{-1}, respectively.

Previously the DNA adduct formation between a reactive α,β-unsaturated aldehyde and guanine was thought to occur via a 1,4-type addition and a direct cyclization of the keto-tautomer of the ring-open adduct, with the cyclization step being rate-determining [24]. The results presented here suggest a 1,2-type addition followed by a tautomerization of the ring-open adduct and cyclization of the enol-tautomer of the ring-open adduct is the kinetically preferred pathway. This new mechanism may partly explain why in single-strand DNA facile cyclization leads to the adduct mainly being present in its ring-closed form.

The ring-closed adduct may form in a number of configurations and conformations. It has been previously shown that only adducts with the same stereochemistry at the two newly formed stereocenters and a trans-orientation of the methyl and hydroxyl substituent are formed [22,59]. The water-catalyzed pathway studied here correctly predicts the transition structure leading to this product to be most stable and a further analysis of the possible conformations of the ring-closed adduct finds that in addition to steric considerations minimal dipole–dipole repulsion together with high $p_N \rightarrow \sigma^*_{C\text{-}O}$ hyperconjugation stabilize the favored configuration and conformation of the adduct.

Acknowledgment

We also acknowledge the system administration support provided by the Faculty of Science at the University of Western Australia to the Linux cluster of the Karton group.

Keywords: DNA damage · water catalysis · Michael addition

How to cite this article: A. A. Kroeger, A. Karton. *J. Comput. Chem.* **2018**, 9999, 1–8. DOI: 10.1002/jcc.25595

Additional Supporting Information may be found in the online version of this article.

[1] K. A. Basu, Int. J. Mol. Sci. **2018**, 19, 970.
[2] T. Pálmai-Pallag, C. Z. Bachrati, Microbes Infect. **2014**, 16, 822.
[3] S. C. Lee, J. C. Chan, Chin Med J. (Engl) **2015**, 128, 1543.
[4] F. Coppedè, L. Migliore, Mutat. Res. **2015**, 776, 84.
[5] L. Wiesmüller, J. M. Ford, R. H. Schiestl, J. Biomed. Biotechnol. **2002**, 2, 45.
[6] I. G. Minko, I. D. Kozekov, T. M. Harris, C. J. Rizzo, R. S. Lloyd, M. P. Stone, Chem. Res. Toxicol. **2009**, 22, 759.
[7] B. U. Islam, R. M. Moinuddin, A. Ali, Int. J. Biol. Macromol. **2014**, 65, 471.
[8] S. S. Hecht, Proc. Natl. Acad. Sci. USA **2006**, 103, 15725.
[9] T. Neudecker, E. Eder, C. Deininger, D. Henschler, Environ. Mol. Mutagen. **1989**, 14, 146.
[10] F.-L. Chung, T. Tanaka, S. S. Hecht, Cancer Res. **1986**, 46, 1285.
[11] C. Czerny, E. Eder, T. M. Rünger, Mutat. Res. **1998**, 407, 125.
[12] S. Stein, Y. Lao, I. Y. Yang, S. S. Hecht, M. Moriya, Mutat. Res. **2006**, 608, 1.
[13] F.-L. Chung, H.-J. Chen, R. G. Nath, Carcinogenesis **1996**, 17, 2105.
[14] E. Demir, B. Kaya, C. Soriano, A. Creus, R. Marcos, Mutat. Res. **2011**, 726, 98.

[15] G.-P. Voulgaridou, I. Anestopoulos, R. Franco, M. I. Panayiotidis, A. Pappa, Mutat. Res. **2011**, 711, 13.
[16] R. G. Nath, J. E. Ocando, J. B. Guttenplan, F.-L. Chung, Cancer Res. **1998**, 58, 581.
[17] M. F. Fracchia, F. J. Schuette, P. K. Mueller, Environ. Sci. Technol. **1967**, 1, 915.
[18] J. A. Theruvathu, P. Jaruga, R. G. Nath, M. Dizdaroglu, P. J. Brooks, Nucleic Acids Res. **2005**, 33, 3513.
[19] P. J. Brooks, J. A. Theruvathu, Alcohol **2005**, 35, 187.
[20] C. de los Santos, T. Zaliznyak, F. Johnson, J. Biol. Chem. **2001**, 276, 9077.
[21] M. P. Stone, Y. J. Cho, H. Huang, H. Y. Kim, I. D. Kozekov, A. Kozekova, H. Wang, I. G. Minko, R. S. Lloyd, T. M. Harris, C. J. Rizzo, Acc. Chem. Res. **2008**, 41, 793.
[22] M. P. Stone, H. Huang, Y.-J. Cho, H.-Y. Kim, I. D. Kozekov, A. Kozekova, H. Wang, I. G. Minko, R. S. Lloyd, T. M. Harris, C. J. Rizzo, In The Chemical Biology of DNA Damage; N. E. Geacintov, S. Broyde, Eds., Wiley: Weinheim, **2010** Ch. 9.
[23] T. E. H. Allen, M. N. Grayson, J. M. Goodman, S. Gutsell, P. J. Russell, J. Chem. Inf. Model. **2018**, 58, 1266.
[24] L. Pardo, R. Osman, H. Weinstein, J. R. Rabinowitz, J. Am. Chem. Soc. **1993**, 115, 8263.
[25] G. B. Desmet, D. R. D'hooge, P. S. Omurtag, P. Espeel, G. B. Marin, F. E. Du Prez, M. F. Reyniers, J. Org. Chem. **2016**, 81, 12291.
[26] D. Xing, L. Sun, R. I. Cukier, Y. Bu, J. Phys. Chem. B **2007**, 111, 5362.
[27] C. Lee, W. Yang, R. G. Parr, Phys. Rev. B **1988**, 37, 785.
[28] A. D. Becke, J. Chem. Phys. **1993**, 98, 5648.
[29] S. Grimme, S. Ehrlich, L. Goerigk, J. Comput. Chem. **2011**, 32, 1456.
[30] J. A. Pople, M. Head-Gordon, K. Raghavachari, J. Chem. Phys. **1987**, 87, 5968.
[31] R. Krishnan, J. S. Binkley, R. Seeger, J. A. Pople, J. Chem. Phys. **1980**, 72, 650.
[32] A. D. McLean, G. S. Chandler, J. Chem. Phys. **1980**, 72, 5639.
[33] C. Gonzalez, H. B. Schlegel, J. Chem. Phys. **1989**, 90, 2154.
[34] C. Gonzalez, H. B. Schlegel, J. Chem. Phys. **1990**, 94, 5523.
[35] S. Kozuch, J. M. L. Martin, J. Comput. Chem. **2013**, 34, 2327.
[36] S. Kozuch, J. M. L. Martin, Phys. Chem. Chem. Phys. **2011**, 13, 20104.
[37] Y. Zhao, N. E. Schultz, D. G. Truhlar, J. Chem. Theory Comput. **2006**, 2, 364.
[38] M. J. Frisch, G. W. Trucks, H. B. Schlegel, G. E. Scuseria, M. A. Robb, J. R. Cheeseman, G. Scalmani, V. Barone, B. Mennucci, G. A. Petersson, H. Nakatsuji, M. Caricato, X. Li, H. P. Hratchian, A. F. Izmaylov, J. Bloino, G. Zheng, J. L. Sonnenberg, M. Hada, M. Ehara, K. Toyota, R. Fukuda, J. Hasegawa, M. Ishida, T. Nakajima, Y. Honda, O. Kitao, H. Nakai, T. Vreven, J. A. Montgomery, Jr.., J. E. Peralta, F. Ogliaro, M. Bearpark, J. J. Heyd, E. Brothers, K. N. Kudin, V. N. Staroverov, T. Keith, R. Kobayashi, J. Normand, K. Raghavachari, A. Rendell, J. C. Burant, S. S. Iyengar, J. Tomasi, M. Cossi, N. Rega, J. M. Millam, M. Klene, J. E. Knox, J. B. Cross, V. Bakken, C. Adamo, J. Jaramillo, R. Gomperts, R. E. Stratmann, O. Yazyev, A. J. Austin, R. Cammi, C. Pomelli, J. W. Ochterski, R. L. Martin, K. Morokuma, V. G. Zakrzewski, G. A. Voth, P. Salvador, J. J. Dannenberg, S. Dapprich, A. D. Daniels, O. Farkas, J. B. Foresman, J. V. Ortiz, J. Cioslowski, D. J. Fox, Gaussian 09, Revision D.01, Gaussian, Inc., Wallingford, CT, **2013**.
[39] M. J. Frisch, G. W. Trucks, H. B. Schlegel, G. E. Scuseria, M. A. Robb, J. R. Cheeseman, G. Scalmani, V. Barone, G. A. Petersson, H. Nakatsuji, X. Li, M. Caricato, A. V. Marenich, J. Bloino, B. G. Janesko, R. Gomperts, B. Mennucci, H. P. Hratchian, J. V. Ortiz, A. F. Izmaylov, J. L. Sonnenberg, D. Williams-Young, F. Ding, F. Lipparini, F. Egidi, J. Goings, B. Peng, A. Petrone, T. Henderson, D. Ranasinghe, V. G. Zakrzewski, J. Gao, N. Rega, G. Zheng, W. Liang, M. Hada, M. Ehara, K. Toyota, R. Fukuda, J. Hasegawa, M. Ishida, T. Nakajima, Y. Honda, O. Kitao, H. Nakai, T. Vreven, K. Throssell, J. A. Montgomery, Jr.., J. E. Peralta, F. Ogliaro, M. J. Bearpark, J. J. Heyd, E. N. Brothers, K. N. Kudin, V. N. Staroverov, T. A. Keith, R. Kobayashi, J. Normand, K. Raghavachari, A. P. Rendell, J. C. Burant, S. S. Iyengar, J. Tomasi, M. Cossi, J. M. Millam, M. Klene, C. Adamo, R. Cammi, J. W. Ochterski, R. L. Martin, K. Morokuma, O. Farkas, J. B. Foresman, D. J. Fox, Gaussian 16, Revision A.03, Gaussian, Inc., Wallingford, CT, **2016**.
[40] J. P. Foster, F. Weinhold, J. Am. Chem. Soc. **1980**, 102, 7211.
[41] F. Weinhold, In Encyclopedia of Computational Chemistry, Vol. 3; P. v. R. Schleyer, N. L. Allinger, T. Clark, J. Gasteiger, P. A. Kollman, H. F. Schaefer, III, P. R. Schreiner, Eds.; Wiley: Chichester, **1998**; pp. 1792–1811.
[42] E. D. Glendening, C. R. Landis, F. Weinhold, WIREs Comput. Mol. Sci. **2012**, 2, 1.
[43] J. E. D. Glendening, K. Badenhoop, A. E. Reed, J. E. Carpenter, J. A. Bohmann, C. M. Morales, C. R. Landis, F. Weinhold, NBO6, Theoretical Chemistry Institute, University of Wisconsin, Madison, WI, **2013**.
[44] C. Y. Legault, CYLview 1.0b, Université de Sherbrooke, Sherbrooke, Canada, **2009**. http://www.cylview.org.
[45] A. A. Kroeger, A. Karton, Aust. J. Chem. **2018**, 71, 212.
[46] F. Sarrami, L.-J. Yu, W. Wan, A. Karton, Chem. Phys. Lett. **2017**, 675, 27.
[47] W. Wan, L.-J. Yu, A. Karton, Aust. J. Chem. **2016**, 69, 943.
[48] A. Karton, Chem. Phys. Lett. **2014**, 592, 330.
[49] J. Y. Shen, W. C. Chao, C. Liu, H. A. Pan, H. C. Yang, C. L. Chen, Y. K. Lan, L. J. Lin, J. S. Wang, J. F. Lu, S. Chun-Wei Chou, K. C. Tang, P. T. Chou, Nat. Commun. **2013**, 4, 2611.
[50] L. Vereecken, J. S. Francisco, Chem. Soc. Rev. **2012**, 41, 6259.
[51] R. S. Assary, P. C. Redfern, J. Greeley, L. A. Curtiss, J. Phys. Chem. B **2011**, 115, 4341.
[52] F. Duarte, A. Toro-Labbé, Mol. Phys. **2010**, 108, 1375.
[53] G. da Silva, Angew. Chem. Int. Ed. **2010**, 49, 7523.
[54] E. Vöhringer-Martinez, B. Hansmann, H. Hernandez, J. S. Francisco, J. Troe, B. Abel, Science **2007**, 315, 497.
[55] D. Seebach, J. Golinski, Helv. Chim. Acta **1981**, 64, 1413.
[56] Y. H. Lam, K. N. Houk, U. Scheffler, R. Mahrwald, J. Am. Chem. Soc. **2012**, 134, 6286.
[57] M. N. Paddon-Row, N. G. Rondan, K. N. Houk, J. Am. Chem. Soc. **1982**, 104, 7162.
[58] A. B. Sanchez, C. C. M. Garcia, F. P. Freitas, G. L. Batista, F. S. Lopes, V. H. Carvalho, G. E. Ronsein, I. G. R. Gutz, P. Di Mascio, M. H. G. Medeiros, Chem. Res. Toxicol. **2018**, 31, 332.
[59] D. W. Boerth, E. Eder, S. Hussain, C. Hoffman, Chem. Res. Toxicol. **1998**, 11, 284.
[60] M. Miljkovic, Carbohydrates: Synthesis, Mechanisms, and Stereoelectronic Effects, Springer, New York, **2009**.

Received: 11 July 2018
Revised: 21 August 2018
Accepted: 23 August 2018